

Uncertainty analysis of downscaling methods in assessing the influence of climate change on hydrology

Fen Ouyang · Haishen Lü · Yonghua Zhu ·
Jianyun Zhang · Zhongbo Yu · Xi Chen ·
Min Li

Published online: 25 September 2013
© Springer-Verlag Berlin Heidelberg 2013

Abstract Five downscaling techniques, namely the statistical downscaling model, the automated statistical downscaling method, the change factor (CF) method, the advanced CF method, the Weather generator (LarsWG5) method, are applied to the upstream basin of the Huaihe River. Changes in regional climate scenarios and hydrology variables are compared in future periods to investigate the uncertainty associated with the downscaling techniques. Paired-sample *T* test is applied to evaluation the significant of the difference of the means between the observed data and the downscaled data in the future. The Xinanjiang rainfall–runoff model is employed to simulate the rainfall–runoff relation. The results demonstrate that the downscaling techniques utilized herein predict an increased tendency in the future. The increases range of maximum temperature (T_{\max}) is between 3.7 and 4.7 °C until the time period of 2070–2099 (2080s). While, the increases range of minimum temperature (T_{\min}) is between 2.8 and 4.9 °C until 2080s. The research presented herein determined that there is an increase predicted for the peaks over threshold (discussed in the paper) and a decrease predicted for the peaks below the threshold (discussed in the paper) in the future, which illustrates that the temperature would rise gradually in the future. Precipitation changes are not as obvious as temperatures changes and

tend to be influence by the season. Most downscaling techniques predict increases, and others indict decreases. The annual mean precipitation range changes between 3.2 and 53.3 %, and moreover, these changes vary from season to season.

Keywords Downscaling · Uncertainty · Climate change · Regional scenarios · Xinanjiang rainfall–runoff model

1 Introduction

The scarcity of water resources caused by environmental pollution and population growth has become an issue of vital importance around the world. Assessing the hydrology and water resources for the future is of great significance for city planning, water resources management and utilization (Gleick 1989; Kiely 1999). General circulation models (herein, referred to as GCMs) provide one of the best tools for simulating current and future prediction of climate change scenarios (Xu 1999). The following steps are used to predict changes in hydrology and water resources: Downscaling the outputs of the GCMs on the global scale into the inputs of the hydrological model on the regional scale to obtain the hydrological response (Christensen et al. 2004; Charlton et al. 2006; Steele-Dunne et al. 2008). There are some mismatch problems between the GCMs and hydrological model (Xu 1999) especially for the spatial and temporal scales, which hampers the development of connectivity between the meteorology and hydrology models. Downscaling technology can be used as a bridge to solve the mismatch problem (Leavesley 1994; Wilby and Wigley 1997; Haylock et al. 2006). There are different downscaling method,

F. Ouyang · H. Lü (✉) · Y. Zhu · Z. Yu · X. Chen · M. Li
State Key Laboratory of Hydrology-Water Resources and
Hydraulic Engineering, College of Hydrology and Water
Resources, Hohai University, Nanjing 210098, China
e-mail: haishenlu@gmail.com

J. Zhang
State Key Laboratory of Hydrology-Water Resources and
Hydraulic Engineering, Nanjing Hydraulic Research Institute,
Nanjing 210029, China

and they can be divided into three categories: statistical downscaling method (Enke and Spekat 1997; Huth 1997; Wilby et al. 2002; Tatli et al. 2004; Feddersen and Andersen 2005), dynamical downscaling method (DÍez et al. 2005; Herrmann and Somot 2008) and statistical-dynamical downscaling method (Conway and Jones 1998; Bárdossy et al. 2002; Boé et al. 2006; Pinto et al. 2010; Najac et al. 2011).

In recent years, several studies have appeared in the literature on the impacts of climate change on hydrology and water resources (Gleick 1989; Arora and Boer 2001; Christensen et al. 2004). These studies indicate that the uncertainty of the downscaling techniques is one of the key areas of research. Many scholars have focused on the uncertainty of the GCMs and greenhouse gases emissions scenarios (herein, referred to as GGES). Merritt et al. (2006) used three GCMs and two emissions scenarios (A2 and B2) to analyze future climate change scenarios. They also utilized the hydrological model (UBC) to obtain the future hydrological response of the upstream portion of the Okanagan basin in Canada. Maurer (2007) applied 11 GCMs to analyze the uncertainty of the impacts of climate change on hydrology and water resources under two emission scenarios (A2 and B1).

Vicuna et al. (2007) studied the sensitivity of climate emissions scenario on water resources. While, Minville et al. (2008) compared annual and seasonal mean discharge, peak discharge and timing of peak discharge of ten different combinations from five GCMs and two emissions scenarios, and then investigated the uncertainty of each of the combinations. Others have investigated the importance and uncertainty of hydrological model in assessing the impact of climate change on hydrology (Ludwig et al. 2009; Bastola et al. 2011). In Ludwig et al. (2009), they compared the complexity of three hydrological models (PROMET, Hydrotel, HSAMI) on the process description, parameter space and spatial and temporal scale. The correction of the climate boundary condition leads to significant changes in the hydrological response. The extension and quantification of uncertainty in the model must be realized in the water resources management. Some studies assessed spatial pattern of urban based on human activities. Qi et al. (2013) utilized an integrated approach to analyze land use/land cover change, spatiotemporal patterns of land fragmentation and variation of ecosystem service value in the context of rapid urbanization. Yue et al. (2012) assessed spatial pattern of urban thermal environment and identified dominant factors to the urban heat island using principal component analysis. These aspects are no doubt important and the uncertainty in the downscaling technique cannot be neglect. Recently, there has been some comparative research carried out on the uncertainty of the downscaling

method (Quintana Seguí et al. 2010; Chen et al. 2011a, b). Regional climate change scenarios are the products of the downscaling processing on GCMs outputs. The different downscaling techniques can provide different results with some results showing that even small fluctuation in the precipitation probability or precipitation intensity producing significant effect on runoff (Risbey and Entekhabi 1996; Whitfield and Cannon 2000). Therefore, the uncertainty of the downscaling technique is one of the major causes of uncertainty in the regional climate change scenarios and hydrological simulation, so it should be paid attention to. Khan et al. (2006a) utilized three downscaling methods [statistical downscaling model (SDSM), LarsWG and artificial neural network (ANN)] to NCEP data and provided a detailed comparison of the differences between current regional climate change scenarios (daily precipitation, maximum and minimum temperatures) generated by three methods, and their uncertainties. There were three downscaling techniques used for CGCM1 in order to produce the future climate change scenarios (Khan et al. 2006b). This provided further validation of the uncertainties in the downscaling techniques; however, their research was not an exhaustive study of all the techniques and their uncertainties. If the regional climate scenarios to the hydrological model are utilized as further input into the models to predict hydrological variables, then it would be able to thoroughly analyze uncertainty in the downscaling techniques. It can also provide a theoretical basis for planning and management of water resources for the future. Chen et al. (2011a) applied six downscaling techniques, which included statistical downscaling methods and dynamical downscaling methods, to investigate the uncertainty in these downscaling techniques. These results were utilized in the Canadian HSAMI hydrological model, which analyzed the annual mean discharge, peak discharge and time to peak discharge, and then compared the uncertainties of the downscaling techniques, GCMs and emission scenarios. Ebrahim et al. (2012) analyzed the uncertainty of three different downscaling techniques (SDSM, Lars-WG and ANN) from two aspects: one is the cognitive uncertainty; while the other one is the inherent uncertainty of random variables.

Several aspects, which include GCMs, emission scenarios, downscaling methods and hydrological models, produce uncertainty, with future investigations taking all these factors into account as much as possible. The main objective of this work is to investigate the uncertainty of downscaling techniques on the upstream portion of Huaihe River basin using five statistical downscaling methods. It will provide new ideas for future researchers.

The layout of this paper is as follows: Sect. 2 gives information on the study area along with the climate and

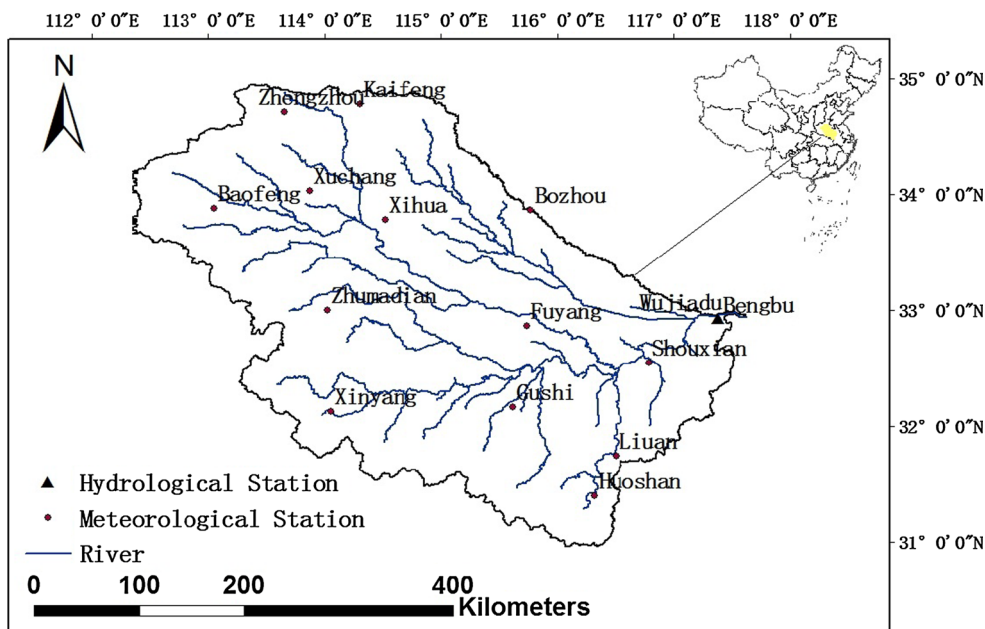
hydrological data; Sect. 3 presents the methods for the downscaling techniques; Sect. 4 provides the results from the different downscaling techniques and the uncertainties produced; which Sect. 5 gives the conclusions with detailed analysis of regional climate change scenarios and hydrological variables for the future.

2 Study area and data

2.1 Study area

The upstream portion of the Huaihe River Basin resides within the latitude and longitude ranges of 112°21′–117°37′E and 30°58′–34°57′N, respectively, and is being utilized in this study (shown in Fig. 1). It is located in the east-central of China, between the Yangtze River and the Yellow River, and the basin area is 121,000 km². The upstream portion of the Huaihe River basin is in the north and south climate transition zone, which has an annual mean precipitation of 900 mm. The precipitation is inter-annual variability, and uneven distribution in the spatial and temporal scales. More than half of the precipitation for the basin occurs during the months of June to September, with the average annual precipitation in the northern region of 600–700 mm, while the southern and western mountainous regions receive about 900–1,400 mm. These areas account for the hilly regions (about 30 %) of the basin area, whereas the plain area account for about 60 % of the basin area. In addition, there are many lakes located on both sides of the Huaihe River, which control the discharge and the runoff to the downstream sections of the river.

Fig. 1 Location map of the upstream portion of the Huaihe River basin



2.2 DATA

The daily meteorological data of this work was derived from China Meteorological Data Sharing Service System <http://cdc.cma.gov.cn/home.do>, which included daily precipitation, daily T_{max} and daily T_{min} for the period of 1961–1990 for 14 meteorological stations (Fig. 1). The daily hydrological data was derived from the China Hydrological Yearbook and included the daily discharge during the period of 1961–1987 for the Wujiadu hydrological station (location shown in Fig. 1). The Wujiadu hydrological station is the main station of the upstream portion of the Huaihe River basin and has a catchment area of 121,000 km².

The daily U.S. National Center for Environmental Prediction (NCEP) data for the period of 1961–1990 were derived from <http://www.cccsn.ca/> and the reanalysis datasets are co-produced by NCEP and U.S. National Center for Atmospheric Research. The most state-of-the-art global data assimilation system and database are applied to reanalyze the observation (OBS) from a variety of sources (such as ground, ship, radiosonde, pilot balloon, aircraft, satellite, etc.).

The daily HadCM3 (abbreviation for Hadley Centre Coupled Model, version 3) (A2) data, for the period of 1961–2099, of the 4th The Intergovernmental Panel on Climate Change (IPCC) was derived from <http://www.cccsn.ca/>. HadCM3 (Gordon et al. 2000) is a coupled ocean–atmosphere model developed by UK Hadley centre in recent years, which is based on the earlier HadCM2 model. HadCM3 has 19 levels (Pope et al. 2000) with a horizontal grid spacing of 2.5° × 3.75°. A2 is one of the emission scenarios of the IPCC’s fourth special report.

IPCC's fourth special report on emission scenarios (SRES) (Nakicenovic et al. 2000) proposed four sets of scenarios called "families": A1, A2, B1 and B2. The A1 family consists of three scenario groups: A1FI (fossil fuel intensive), A1B (balance) and A1T (predominantly non-fossil fuel). This paper will concentrate on A2, which describes a very heterogeneous world. The theme is self-reliance, and the protection of regional identity. The emphasis is on family values and local traditions. Birth rates between the different regions are not the same, which result in the continued growth of the global population. The A2 scenarios assume a high population growth, which results in higher emission.

This study covers the period 1961–1990 for the base years (denoted by 1980s) and covers the three future periods: 2010–2039, 2040–2069 and 2070–2099 for the future years (denoted by 2020s, 2050s and 2080s, respectively).

3 Methodology

3.1 Downscaling methods

3.1.1 Statistical downscaling model-based method

The SDSM-based method is a decision support tool for assessing regional climate change scenarios, which has been developed by Wilby et al. (1999; 2002; 2003). SDSM has now been used widely in worldwide applications (Wilby et al. 2002, 2003; Dibike and Coulibaly 2005; Khan et al. 2006a; Chu et al. 2010). The main procedures are as following:

- (1) *Screen predictions* identifying the empirical relationships between gridded predictors and single site predictands (Wilby et al. 2002). The variables that showed significantly correlated to the predictands were selected as the predictors (Chen et al. 2011a).
- (2) *Set model structure and calibrate model* steps utilized here are: (a) multiple linear regression equations were established for each month, (b) the parameters of the regression model were obtained via the dual simplex optimization algorithm, and (c) the most parsimonious model of the predictand were selected according to Akaike's Information Criterion.
- (3) *Weather generator* produce ensembles of synthetic daily weather series according to the NCEP re-analysis atmospheric predictors for the base years and the multiple regression models.
- (4) *Generate scenario* produce ensembles of synthetic daily weather series according to the GCM atmospheric predictors and the multiple regression model

for the base years (1980s) and the future years (2020s, 2050s and 2080s).

3.1.2 Automated statistical downscaling (ASD) method

The ASD method (Khan et al. 2006a; Hessami et al. 2008) was developed to improve the spatial resolution of the GCM outputs and has been developed in the Matlab environment. The ASD method is the advanced SDSM method. In the ASD method, a stepwise linear regression approach is applied to select predictors, variance inflation and bias correction were set automatically, and multiple linear regressions were used in model calibration.

Temperature (i.e. T_{\max} and T_{\min}) can be modeled in one step owing to the direct relationship of the predictor–predictand. Precipitation has an indirect relationship with the predictors. Hence, judging precipitation occurrence before calculating precipitation amounts.

3.1.3 Change factor (CF) method

The CF method (Hay et al. 2000; Diaz-Nieto and Wilby 2005) is an ordinary bias correction method. The CF method is often used to eliminate or reduce the bias between the model outputs and OBSs. The main procedures of the CF method are modifying the daily time series of the variables (i.e. precipitation and temperature) in the future years (2020s, 2050s and 2080s) by adding the monthly mean changes of GCM outputs. The modified daily temperature (T_{\max} and T_{\min}) for the future years is obtained by adding the monthly changes between the future years and the base years of GCM, while the modified daily precipitation for the future years is obtained by multiplying the ratio with the daily precipitation of the base years. The adjusted formula for modified daily temperature (T_{\max} and T_{\min}) is expressed in Eq. (1), and the modified daily precipitation is expressed in Eq. (2):

$$T_{adj, fur, d} = T_{obs, d} + \sum_{i=1}^k p_i (\bar{T}_{GCM, fur, m} - \bar{T}_{GCM, ref, m}) \quad (1)$$

$$P_{adj, fur, d} = P_{obs, d} \times \sum_{i=1}^k p_i (\bar{P}_{GCM, fur, m} / \bar{P}_{GCM, ref, m}) \quad (2)$$

where $T_{adj, fur, d}$ is the adjusted daily temperature (T_{\max} and T_{\min}) for the future years (2020s, 2050s and 2080s), $T_{obs, d}$ is the observed daily temperature for the base years (1980s), $\bar{T}_{GCM, fur, m}$ is the monthly mean temperature of the GCM outputs for the future years, $\bar{T}_{GCM, ref, m}$ is the monthly mean temperature of the GCM outputs for the base years, p_i is the weight of each grid cell and k is the number of the grid cells.

3.1.4 Advanced CF (AdvCF) method

The AdvCF method is inspired by the CF method and it is a combination of spatial interpolation and CF method. In this method, the inverse distance squared weighted interpolation method (IDW) was utilized to interpolate the temperature or precipitation of the GCM outputs with a resolution of $k \times k$ grid cells into a resolution of $(2k - 1) \times (2k - 1)$ grid cells, and then CF method is used to downscale the temperature or precipitation further:

$$y = \frac{\sum_1^k \frac{1}{d_i^2} x_i}{\sum_1^k \frac{1}{d_i^2}} \tag{3}$$

where y is the interpolated data (either temperature or precipitation), x_i is i th $i = 1, 2, \dots, k$ point of the sample, d_i is the distance between i th point and the interpolated data.

$$T_{adj,fur,d} = T_{obs,d} + \sum_{i=1}^{2k-1} p_i (\bar{T}_{GCM^*,fur,m} - \bar{T}_{GCM^*,ref,m}) \tag{4}$$

$$P_{adj,fur,d} = P_{obs,d} \times \sum_{i=1}^{2k-1} p_i (\bar{P}_{GCM^*,fur,m} / \bar{P}_{GCM^*,ref,m}) \tag{5}$$

where $\bar{T}_{GCM^*,fur,m}$ and $\bar{T}_{GCM^*,ref,m}$ are interpolated monthly mean temperature for the future years (2020s, 2050s and 2080s) and the base years (1980s), respectively; $\bar{P}_{GCM^*,fur,m}$ and $\bar{P}_{GCM^*,ref,m}$ are the interpolated monthly mean precipitation for the future years and base year, respectively.

3.1.5 Weather generator (LarsWG5) method

LarsWG5 is a stochastic weather generator developed by the Rothamsted Research of UK in 2010 and it is based on the series weather generator discussed in 1991 (Racsko et al. 1991). LarsWG5 can be used to generate the climate scenarios (precipitation, T_{max} , T_{min} and solar radiation) for the current and future applications. The LarsWG5 method provides data in time series at each site.

A semi-empirical distribution model was used in LarsWG5 (Semenov et al. 1998; Khan et al. 2006a, b) to simulate the dry and wet spell length, daily precipitation and daily solar radiation, which allow the method to overcome the problems associated with the Markov chain.

For the LarsWG5 method, the temperature (T_{max} and T_{min}) and precipitation are different in their solution schemes. The temperatures are obtained with the stochastic process, which utilizes a finite Fourier series of third-order to simulate the seasonal cycles of mean and standard deviations; while, the normal distribution is applied to model the residuals.

3.2 Hydrological model

The Xinanjiang model is a conceptual rainfall–runoff model (denoted by XAJ-RR model), which was proposed in 1980 (Zhao et al. 1980) and developed in 1992 (Zhao 1992) by combining with stored-full runoff theory. The XAJ-RR model has been widely used to forecast flood in large basins of the humid and semi-humid regions of China (Lü et al. 2013). The model structure is shown in Fig. 2; while, Table 1 presents the parameters and their physical meanings in the XAJ-RR model. The model utilizes 15 parameters, including five evapotranspiration component parameters (K, WUM, WLM, WDM, C), six runoff production parameters (B, IMP, SM, EX, KG, KSS), three runoff concentration parameters (KKG, KKSS, CS), and the unit hydrograph (UH). The model structure and calculation is divided into four parts (Zhao 1992): evapotranspiration, runoff production, runoff separation, and flow concentration. The basin evapotranspiration are calculated in accordance to the three layers-evapotranspiration model.

In the evapotranspiration model, the measured pan evaporation (EM) is replaced by the potential evapotranspiration (ET_p) (Wang et al. 2009) due to the lack of future evapotranspiration. In order to avoid any bias resulting from potential evapotranspiration, ET_p were calculated in the current and future as follows:

$$ET_p = 0.0023 \times (T_{mean} + 17.8) \times (T_{max} - T_{min})^{0.5} \times Ra \tag{6}$$

where ET_p is daily potential evapotranspiration, T_{mean} is daily mean temperature, T_{max} and T_{min} are maximum and minimum daily temperature, respectively, and Ra is extraterrestrial radiation (Hargreaves and Samani 1982).

The XAJ-RR model is applied herein at the monthly scale with the model utilizing the monthly precipitation and monthly potential evapotranspiration information. The model provides monthly discharge values for the simulation output. The optimal combination of parameters was chosen based on the following object functions:

$$NS = 1 - \frac{\sum_{i=1}^m (Q_{obs,i} - Q_{sim,i})^2}{\sum_{i=1}^m (Q_{obs,i} - \bar{Q}_{sim})^2} \tag{7}$$

$$ER = \frac{\sum_{i=1}^m (Q_{obs,i} - Q_{sim,i})}{\sum_{i=1}^m Q_{obs,i}} \tag{8}$$

$$RSME = \sqrt{\frac{i}{m} \sum_{i=1}^m (Q_{obs,i} - Q_{sim,i})^2} \tag{9}$$

$$R = \frac{\sum_{i=1}^m (Q_{obs,i} - \bar{Q}_{obs})(Q_{sim,i} - \bar{Q}_{sim})}{\sqrt{\sum_{i=1}^m (Q_{obs,i} - \bar{Q}_{obs})^2} \sqrt{\sum_{i=1}^m (Q_{sim,i} - \bar{Q}_{sim})^2}} \tag{10}$$

Fig. 2 Flow chart of the XAJ-RR model. Table 1 gives the definitions of each of the parameters given in this flowchart

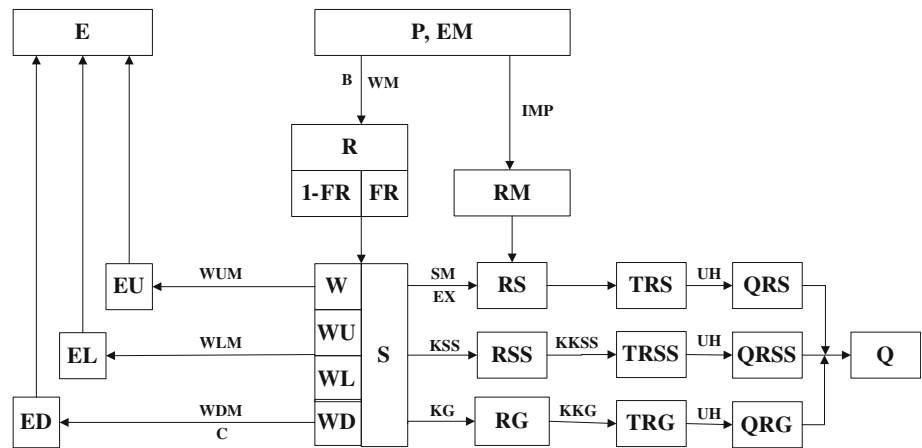


Table 1 Parameters of the XAJ-RR model

| Parameter | Physical meaning | Unit |
|-----------|--------------------------------------------------------------------|------|
| B | Exponential of the distribution of tension water capacity | – |
| WUM | Averaged soil moisture storage capacity of the upper layer | mm |
| WLM | Averaged soil moisture storage capacity of the lower layer | mm |
| WDM | Averaged soil moisture storage capacity of the deep layer | mm |
| K | Ratio of potential evapotranspiration to pan evaporation | – |
| C | Evapotranspiration coefficient of deeper layer | – |
| IMP | Ratio of impervious area to the total area of the basin | % |
| SM | Free water storage capacity | – |
| EX | Exponential of distribution water capacity | mm |
| KSS | Out flow coefficient of free water storage to the inter flow | – |
| KG | Out flow coefficient of free water storage to the groundwater flow | – |
| KKSS | Recession constant of lower interflow storage | – |
| KKG | Recession constant of groundwater storage | – |
| CS | Recession constant of channel network storage | – |
| UH | Unit hydrograph | – |

where *NS* is Nash–Sutcliffe efficiency coefficient, *ER* is the total discharge error, *RSME* is mean square deviation; *R* is correlation coefficient, *m* is the length of the monthly time series, $Q_{obs,i}$ is the OBS of monthly discharge, $Q_{sim,i}$ is the simulation of monthly discharge, $\bar{Q}_{obs,i}$ is the OBS of mean discharge for the chosen period, and \bar{Q}_{sim} is the simulation of mean discharge for the same period. A value near one for the Nash–Sutcliffe efficiency coefficient indicates that the parameters utilized in the simulations are optimal and that the results produced are close to the OBSs. While with the total discharge error, a value close to zero is ideal for the parameter combination to be optimal.

3.3 Uncertainty assessment in downscaled results

Some basic sample statistics are, for instance, sample means, sample median, sample standard deviation etc. Of course, a summary statistic like the sample mean will fluctuate from

sample to sample and a statistician would like to know the magnitude of these fluctuations around the corresponding sample parameter (Singh and Xie 2008). Non-parametric test for the difference means of two samples are used to solve this issue. One of the best non-parametric methods for constructing a hypothesis test *p* value for $\mu_1 - \mu_2$ (difference of means between observed data and downscaled data) is paired-sample *T*-test. The *T* test is also known as the student test. In terms of hypothesis testing, the *p* value is the level of significance for which the observed test statistic lies on the boundary between acceptance and rejection of the null hypothesis. At any significance level larger than the *p* value one rejects the null hypothesis, and at any significance level less than the *p* value one accepts the null hypothesis. Paired-samples *T*-test is used to test two related samples that represented by the unknown sample means whether there is a difference.

The basic steps of paired-sample *T*-test for significant test of sample means difference are as follows:

propose null-hypothesis and alternative hypothesis

$$H_A : \mu_d \neq 0, H_0 : \mu_d = 0 \tag{11}$$

$$\mu_d = \mu_1 - \mu_2 \tag{12}$$

where μ_d is the difference mean between the two sample.

The null-hypothesis equivalent to:

$$H_A : \mu_1 \neq \mu_2, H_0 : \mu_1 = \mu_2 \tag{13}$$

calculate t value as following:

$$t = \frac{\bar{d}}{S_{\bar{d}}}, df = n - 1 \tag{14}$$

$$S_{\bar{d}} = \frac{S_d}{\sqrt{n}} = \sqrt{\frac{\sum_{j=1}^n (d_j - \bar{d})^2}{n(n-1)}} \tag{15}$$

$$d_j = x_{1j} - x_{2j} \tag{16}$$

$$\bar{d} = \sum_{j=1}^n d_j / n \tag{17}$$

where d_j is the difference between each pair of data of two sample; $S_{\bar{d}}$ is standard error of d_j , n is the number repeated test; x_{1j} are observed data and x_{2j} are downscaled ones.

lookup table for the p value based on df and test level, and then make statistical inference.

4 Results

4.1 Calibration and validation of hydrological model

The calibration of the parameters is a significant step in utilizing the XAJ-RR model in these studies. Observed discharge values from the years of 1961–1972 (11 years) were utilized in the calibration process of the model; while, the observed discharge from the years of 1974–1976 and 1980–1987 were utilized to validate the model. The XAJ-RR model herein was applied to the Wujiadu hydrological control station and utilized in simulations over a monthly basis. Trial and error was employed in the calibration of the model parameters. The analysis of statistical characteristics for the calibration period and validation period are list in Table 2.

The simulated results for both the calibration and validation periods are presented in Fig. 3. The flow hydrograph results presented in Fig. 3 indicate that the XAJ-RR model performs well at Wujiadu station; however, it does show that the model has problems capturing the peak discharge values at this station. The problems in capturing the peak discharge values may be due to some man-made reservoirs that are located in the upper reaches of the river. Therefore, it is a non-negligible factor for the difference between the observational data and the model results. It should also be noted that the temporal scale is also affected in the model

results. As one might expect, the monthly model shows poorer results than the daily and the hourly model. Figure 3 shows that the validation results capture the observed data as well as the calibration results.

4.2 Climate change scenarios

4.2.1 Monthly mean T_{max} and T_{min}

Figure 4 shows the monthly mean temperature (T_{max} and T_{min}) of the five downscaling methods discussed earlier in Sect. 3 for the future years (2020s, 2050s and 2080s) and the OBS for the base years (1980s). For each variable (T_{max} and T_{min}), the results show that all methods have an increasing trend in the three future years scenarios.

For all the future year scenarios, the results show that each of the downscaling methods obtains an increase in the mean T_{max} as compared with the OBSs. These increases in the annual mean T_{max} range between 1.0 and 1.2 °C for 2020s. In the first panel of Fig. 4, the greatest increase in the annual mean T_{max} occurs when using the AdvCF method, while the annual mean T_{max} increases the least with the LarsWG5 method. When analyzing the result for 2050s, it was determined that the annual mean T_{max} increases from 2.0 to 2.5 °C. For these results, the LarsWG5 method produced the greatest increase in annual mean T_{max} and the ASD method produced the smallest increase in the annual mean T_{max} . For the 2080s, the annual mean T_{max} increases vary from 3.7 to 4.7 °C with the trends showing similar results to those of the 2050s results—most significant increase was found with the LarsWG5 method and the smallest increase predicted with the ASD method. Similar results were obtained with the annual mean T_{min} in the future periods, with the increases ranging between 0.5 and 1.1 °C for 2020s, 1.5 and 2.7 °C for 2050s, and 2.8 and 4.9 °C for 2080s. For the annual mean T_{min} values in all the future periods, the most significant increases in temperature and the smallest increases in temperature were predicted by the LarsWG5 and ASD, respectively.

The variation in the temperature range is different depending on the month of the year. The largest increases in the temperature occur in July and August, while December and January produce the lowest temperature changes. In the next 90 years, all the downscaling methods show an increase in the range of T_{max} of 2.1–4.2 °C for the month of January, 3.1–4.2 °C for the month of December, 4.5–8.8 °C for the month of July and 5.4–6.6 °C for the month of August. T_{min} shows a range that increase less than the range of T_{max} . The five downscaling methods produce increases in the temperature ranges between 1.4 and 4.3 °C for January, 2.2 and 4.3 °C for December, 4.3 and 5.5 °C for July, and 3.4 and 5.7 °C for August. Overall, the

Table 2 Analysis of statistical characteristics

| | NS | ER | RSME | R |
|--------------------|--------|---------|--------|--------|
| Calibration period | 0.7095 | −0.0294 | 567.97 | 0.8430 |
| Validation period | 0.7621 | 0.0023 | 561.50 | 0.8757 |

Fig. 3 Parameters calibration and validation for the XAJ-RR model during the base years (1961–1990). In the upper figure, the abscissa shows 132 months for 11 years (1961.01–1972.12). In the lower figure, the abscissa shows 132 months for 11 years (1974.01–1976.12 and 1980.01–1987.12)

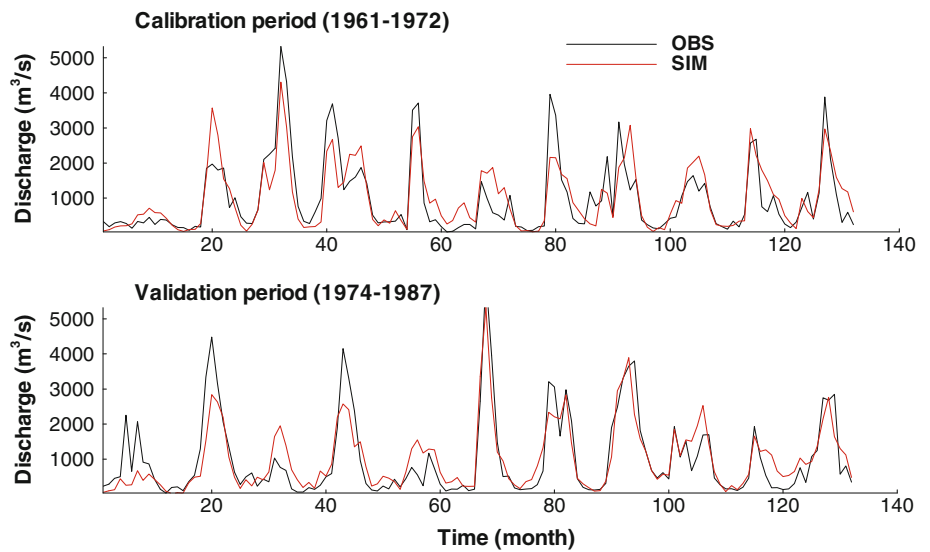
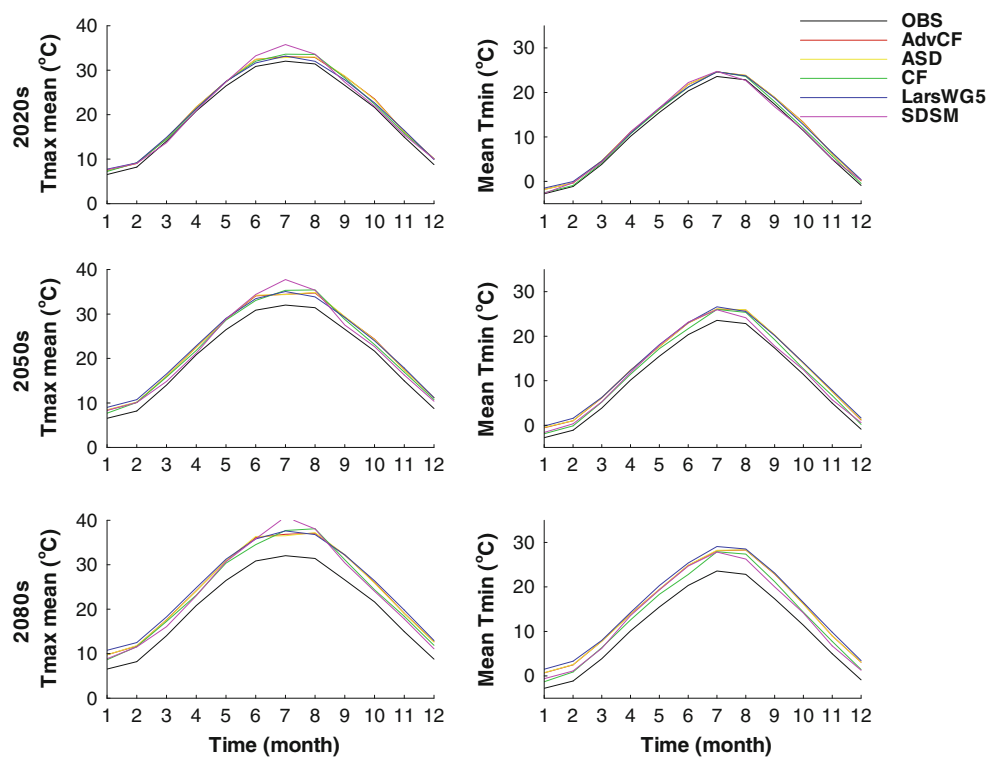


Fig. 4 Observed and predicted mean temperature (T_{max} and T_{min}) of the base years (1980s) and the future year (2020s, 2050s and 2080s) at upstream portion of the Huaihe River basin



LarsWG5 method predicts the largest temperature increases in the future, while ASD predicts the smallest temperature increases.

Figure 5 presents the average monthly peaks over threshold (POT) and average monthly peaks below threshold (PBT), which describe the temperature change in

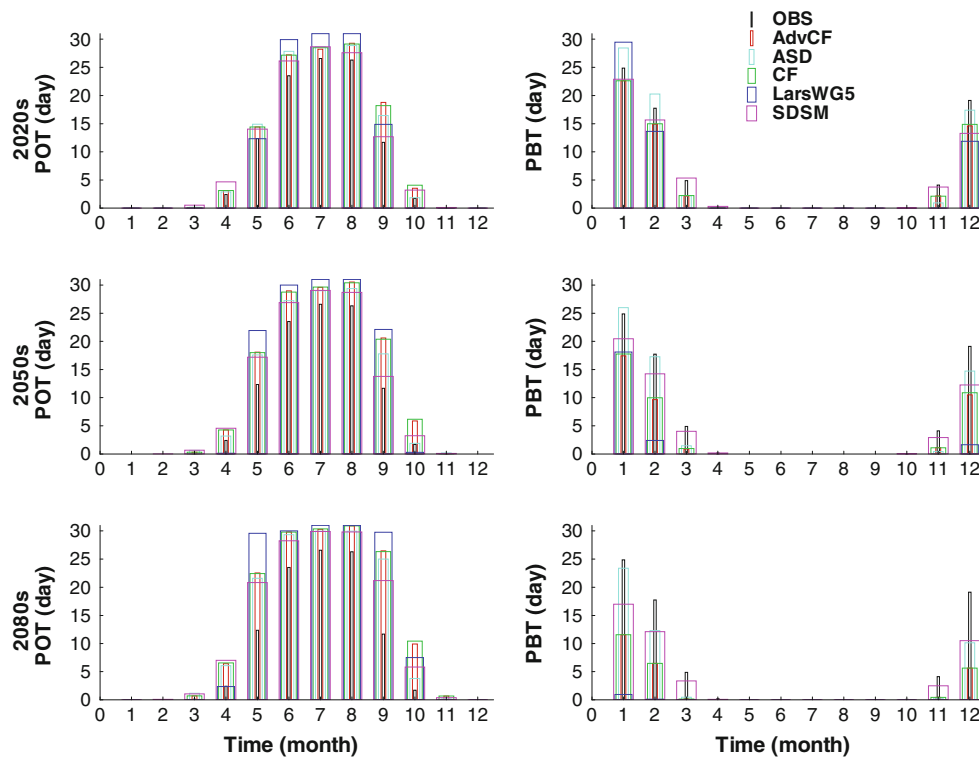


Fig. 5 POT and PBT for the base years (1980s, shown as OBS data) and the future years (2020s, 2050s and 2080s)

the future years (2020s, 2050s, and 2080s) compared with the base years (1980s, the OBS data in Fig. 5). The POT provides a count of the average number of days that the maximum temperature is greater than a specified threshold (set to 28 °C for the studies herein) in each month for the given period of time. While, the PBT provides a count of the average number of days that the minimum temperature falls below a specified threshold (set to 0 °C for the studies herein). These results indicate that all the downscaling methods obtain an increase in the POT and a decrease in the PBT in different extent, respectively. Results from Fig. 5 indicate that the average annual POT was 92.3 days for the base years (1980s, shown as the observed data), while the results from each of the downscaling methods show the following average annual POT for each of the future years (2020s, 2050s, and 2080s): 124.6, 137.9 and 157.7 days for the AdvCF method; 121.7, 126.8 and 147 days for the ASD method; 124.6, 137.9 and 158.1 days for the CF method; 119.1, 125.5 and 161.2 days for the LarsWG5 method; and 117.4, 138.2 and 116 days for the SDSM method. From these results, it can be seen that the POT increases gradually during the future years.

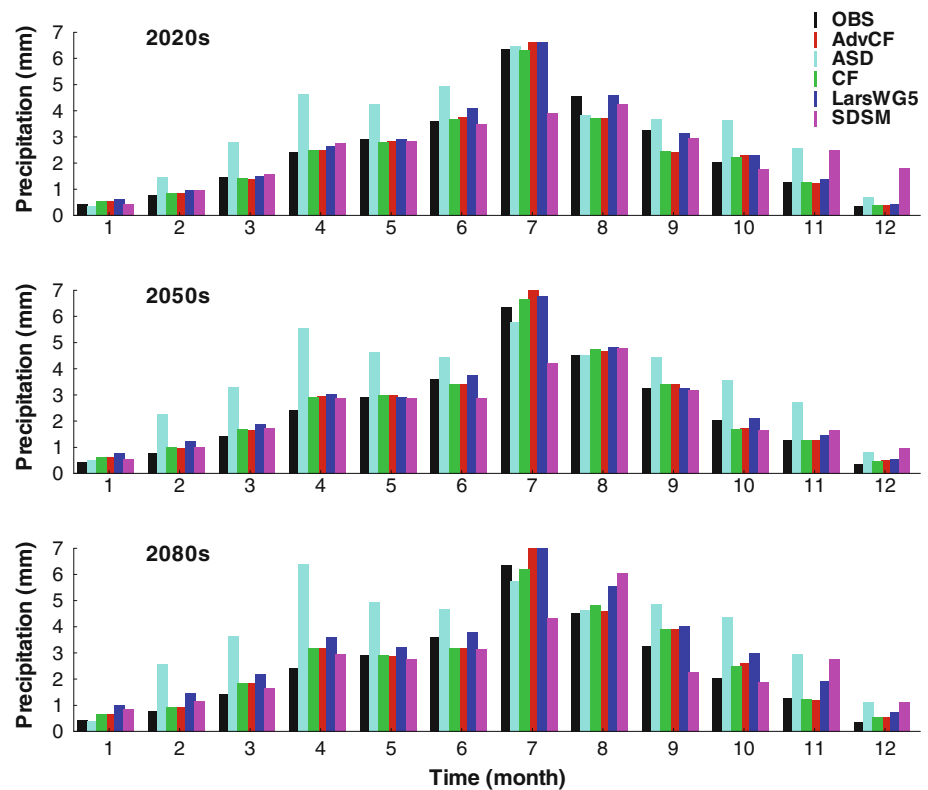
From Fig. 5, it can be seen that there is an opposite trend in the PBT results as compared to the POT during the future years. Results show that the average annual PBT for the base years was 70.9 days, while the average annual PBT for the future years (2020s, 2050s, and 2080s) for the

five downscaling methods are as follows: 56.3, 39 and 24.2 days for the AdvCF method; 69.1, 59.5 and 46.6 days for the ASD method; 56.8, 40.7 and 24.2 days for the CF method; 55, 22.1 and 1.1 days for the LarsWG5 method; 61.2, 54.4, and 45.5 days for the SDSM method. In summary, the results show that the PBT decreases gradually over the future years. Thus, the results from the POT and PBT demonstrate that the temperature would increase gradually in the future years.

4.2.2 Mean precipitation

Figure 6 displays the mean daily precipitation for both future and base year. The trends in the precipitation changes are not determined using the same methods as those presented with the temperature changes. Results show that the changes in precipitation amounts increase for some months of the year, while it decreases for the other months of the year. The changes in precipitation vary depending on the month of the year and the method of downscaling. All the downscaling methods produce large changes in the precipitation during the winter months (between November and April); while, the changes in precipitation are small during the summer months (between March and October). Herein, the results from July and December are utilized to discuss the results shown in Fig. 5. The five downscaling methods generate

Fig. 6 Mean daily precipitation for the base years (1980s, shown as the OBS data) and the future years (2020s, 2050s and 2080s) at the upstream portions of the Huaihe River basin



precipitation changes in July that vary between -38.1 and 4.4 % for 2020s, -33.3 and 11.9 % for 2050s, -31.8 and 16.8 % for 2080s. While in December, the downscaling methods generate changes in precipitation between 0.8 and 375.3 % for 2020s, 27.6 % and 111.2 % for 2050s, 44.9 and 201.5 % for 2080s. ASD provides the largest increase in the precipitation changes in the future periods, especially in the months of February, March, April, November and December. For example, ASD shows an increase in the precipitation changes during April of 92.1 , 129.5 and 164.5 % for the future years (2020s, 2050s and 2080s), respectively.

For the annual mean daily precipitation, the five downscaling methods predict changes that range from -4.5 % (CF method) to 36.4 % (ASD method) for 2020s, from 3.7 % (SDSM method) to 48.4 % (ASD method) for 2050s and from 4.7 % (SDSM method) to 61.7 % (ASD method) for 2080s.

In view of the obvious seasonal changes of the watershed hydrology and water resources, the regional climate change scenarios are analyzed seasonally. Figure 7 presents scatter plots of T_{\max} and seasonal changes in the precipitation for the future years.

Figure 7 shows that the predicted T_{\max} increases for all of the downscaling methods during all of the seasons. The significant increases in temperature range between 0.2 and 2.8 °C for 2020s and from 2.7 to 6.8 °C for 2080s. In

general, the temperature increases are largest in the summer for each of the future years.

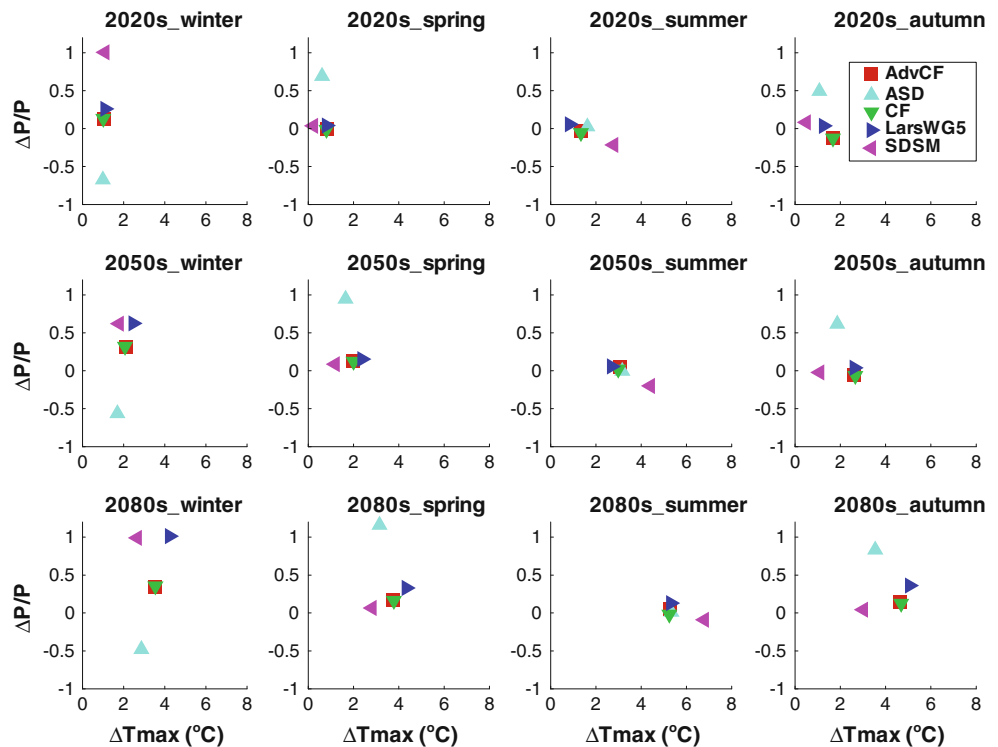
For the total precipitation, the five downscaling methods show significant seasonal variability, with the most notable variability for the ASD method. However, total precipitation changes are not significant in the summer months for the ASD method, which show changes of 4.6 , 0.5 and 1.2 % for the future years (2020s, 2050s and 2080s), respectively. In contrast, the total precipitation changes in a significantly during the other seasons for each of the future years (i.e. -67.2 , -56.2 and -47.7 % in winter seasons, 69.2 , 94.6 and 115.9 % in spring seasons and 49.3 , 61.8 and 83.2 % in autumn seasons).

For the three future periods, the downscaling methods produce seasonal increases in the total precipitation with an ordinal order of winter, autumn, spring and summer. CF method and AdvCF method result in smaller increases in total precipitation as compared to the other downscaling methods in the spring, summer and autumn of 2020s, with the AdvCF method producing the smallest changes in total precipitation for each season.

4.2.3 Error evaluation in the estimates of means

The comparative plots of the means of daily precipitation, T_{\max} and T_{\min} of observed for the base years and down-scaled for the future years have been analysed in Sects.

Fig. 7 Season changes for T_{max} and total precipitation of the future years (2020s, 2050s and 2080s) comparison with the base years (1980s, shown as the OBS data)



4.2.1 and 4.2.2. In this section, all the difference between observed data and the downscaled data are tested at the 95 % confidence level based on the paired-sample *T*-test. The *p* values of the *T*-test for the difference of the observed and downscaled via five downscaling methods are shown in Tables 3, 4, and 5 respectively for daily precipitation, daily T_{max} and daily T_{min} .

Table 3 shows the statistical significance test results (*p* value) of difference between observed and downscaled daily precipitation for the three future periods. For 2020s, the difference produced by AdvCF method and CF method are significant ($p < 0.05$) in all 12 months; the ASD method results show significant in 9 months; and the LarsWG5 method and SDSM results show significant in 2 months. For 2050s, similar results are obtained by AdvCF method and CF method. The ASD method results are significant in 9 months. The LarsWG5 results are significant in 5 months and the SDSM results are significant in 8 months. For 2080s, the same results are obtained by AdvCF and CF method. The results of ASD method and LarsWG5 method are significant in 9 months. The results are significant in 7 months produced by SDSM. In generally speaking, the trend of errors in daily precipitation downscaled via five downscaling methods for the future years (2020s, 2050s and 2080s) are significant in most of months. The most significant is AdvCF method and CF method, whose errors are not insignificant in any of month. And the errors of other three methods are

insignificant in only a few months. It indicates that the choice of downscaling methods will affect the results of the regional scenarios. The results obtained by any of downscaling methods are not completely accurate. All the downscaling methods contain uncertainties.

Table 4 shows the significant results (*p* value) of the paired-sample *T*-test in daily T_{max} at the 95 % confidence level. The test results for the difference of means between observed data and the downscaled data for the future years are significant ($p < 0.05$) in most of the months for all the downscaling methods. Only ASD methods errors are insignificant in two months in 2020s, and SDSM methods errors are insignificant in 3 months in 2020s and 1 month in 2050s. All the downscaling methods errors are significant in all of the months in 2080s. For the daily T_{min} , the results of the five methods predict the similar level. The Table 5 shows *p* value of the paired-sample *T*-test in T_{min} . For 2020s, Only ASD errors are insignificant in 1 month and SDSM errors are insignificant in three months. AdvCF method, CF method and LarsWG5 method errors are significant in all 12 months. All of the five methods errors are significant in all the 12 months for the 2050s and 2080s. Based on this evolution, all five downscaling methods are similar at 95 % confidence level for daily T_{max} and T_{min} . But the SDSM method and ASD method generate the least errors. AdvCF method, CF method and LarsWG5 errors are significant in all the future months.

Table 3 Results (p value) of the T test for the equality means of the observed and downscaled daily T_{\max} at the 95 % confidence level

| Period | Month | p value | | | | |
|--------|-------|-----------|-------|-------|-------|---------|
| | | AdvCF | CF | ASD | SDSM | LarsWG5 |
| 2020s | Jan | 0.000 | 0.000 | 0.001 | 0.000 | 0.000 |
| | Feb | 0.000 | 0.000 | 0.000 | 0.002 | 0.000 |
| | Mar | 0.000 | 0.000 | 0.080 | 0.244 | 0.000 |
| | Apr | 0.000 | 0.000 | 0.051 | 0.661 | 0.000 |
| | May | 0.000 | 0.000 | 0.000 | 0.000 | 0.000 |
| | Jun | 0.000 | 0.000 | 0.000 | 0.000 | 0.000 |
| | Jul | 0.000 | 0.000 | 0.000 | 0.000 | 0.000 |
| | Aug | 0.000 | 0.000 | 0.000 | 0.000 | 0.000 |
| | Sep | 0.000 | 0.000 | 0.000 | 0.000 | 0.000 |
| | Oct | 0.000 | 0.000 | 0.000 | 0.104 | 0.000 |
| | Nov | 0.000 | 0.000 | 0.000 | 0.008 | 0.000 |
| | Dec | 0.000 | 0.000 | 0.000 | 0.000 | 0.000 |
| 2050s | Jan | 0.000 | 0.000 | 0.000 | 0.000 | 0.000 |
| | Feb | 0.000 | 0.000 | 0.000 | 0.000 | 0.000 |
| | Mar | 0.000 | 0.000 | 0.000 | 0.006 | 0.000 |
| | Apr | 0.000 | 0.000 | 0.000 | 0.121 | 0.000 |
| | May | 0.000 | 0.000 | 0.000 | 0.000 | 0.000 |
| | Jun | 0.000 | 0.000 | 0.000 | 0.000 | 0.000 |
| | Jul | 0.000 | 0.000 | 0.000 | 0.000 | 0.000 |
| | Aug | 0.000 | 0.000 | 0.000 | 0.000 | 0.000 |
| | Sep | 0.000 | 0.000 | 0.000 | 0.000 | 0.000 |
| | Oct | 0.000 | 0.000 | 0.000 | 0.000 | 0.000 |
| | Nov | 0.000 | 0.000 | 0.000 | 0.000 | 0.000 |
| | Dec | 0.000 | 0.000 | 0.000 | 0.000 | 0.000 |
| 2080s | Jan | 0.000 | 0.000 | 0.000 | 0.000 | 0.000 |
| | Feb | 0.000 | 0.000 | 0.000 | 0.000 | 0.000 |
| | Mar | 0.000 | 0.000 | 0.000 | 0.000 | 0.000 |
| | Apr | 0.000 | 0.000 | 0.000 | 0.000 | 0.000 |
| | May | 0.000 | 0.000 | 0.000 | 0.000 | 0.000 |
| | Jun | 0.000 | 0.000 | 0.000 | 0.000 | 0.000 |
| | Jul | 0.000 | 0.000 | 0.000 | 0.000 | 0.000 |
| | Aug | 0.000 | 0.000 | 0.000 | 0.000 | 0.000 |
| | Sep | 0.000 | 0.000 | 0.000 | 0.000 | 0.000 |
| | Oct | 0.000 | 0.000 | 0.000 | 0.000 | 0.000 |
| | Nov | 0.000 | 0.000 | 0.000 | 0.000 | 0.000 |
| | Dec | 0.000 | 0.000 | 0.000 | 0.000 | 0.000 |

4.2.4 Uncertainty of annual precipitation and T_{\max} and T_{\min}

The probability density functions (PDFs) of the annual precipitation, T_{\max} and T_{\min} are used to show the uncertainties in the downscaling methods (shown in Fig. 8). The PDF of each variable (precipitation, T_{\max} or T_{\min}) are presented according to the mean and variance for each future period, respectively. Figure 8 shows the PDFs for

each variable and each future period. For all the predictands, the differences between the results of the five downscaling methods increase with time.

The annual mean precipitation for the base years (1980s) in Fig. 8 is represented by a black line, which has a median value of 900.8 mm and a variance value of 168.6 mm². The ASD method shows the most significant increase in the median value with the following values: 1179 mm for 2020s, 1271 mm for 2050s and 1381 mm for 2080s. These

Table 4 Results (*p* value) of the *T* test for the equality means of the observed and downscaled daily T_{\min} at the 95 % confidence level

| Period | Month | <i>p</i> value | | | | |
|--------|-------|----------------|-------|-------|-------|---------|
| | | AdvCF | CF | ASD | SDSM | LarsWG5 |
| 2020s | Jan | 0.000 | 0.000 | 0.016 | 0.000 | 0.000 |
| | Feb | 0.000 | 0.000 | 0.277 | 0.000 | 0.000 |
| | Mar | 0.000 | 0.000 | 0.033 | 0.003 | 0.000 |
| | Apr | 0.000 | 0.000 | 0.000 | 0.000 | 0.000 |
| | May | 0.000 | 0.000 | 0.000 | 0.000 | 0.000 |
| | Jun | 0.000 | 0.000 | 0.000 | 0.000 | 0.000 |
| | Jul | 0.000 | 0.000 | 0.000 | 0.000 | 0.000 |
| | Aug | 0.000 | 0.000 | 0.000 | 0.176 | 0.000 |
| | Sep | 0.000 | 0.000 | 0.000 | 0.000 | 0.000 |
| | Oct | 0.000 | 0.000 | 0.000 | 0.241 | 0.000 |
| | Nov | 0.000 | 0.000 | 0.000 | 0.577 | 0.000 |
| | Dec | 0.000 | 0.000 | 0.000 | 0.000 | 0.000 |
| 2050s | Jan | 0.000 | 0.000 | 0.000 | 0.000 | 0.000 |
| | Feb | 0.000 | 0.000 | 0.000 | 0.000 | 0.000 |
| | Mar | 0.000 | 0.000 | 0.000 | 0.000 | 0.000 |
| | Apr | 0.000 | 0.000 | 0.000 | 0.000 | 0.000 |
| | May | 0.000 | 0.000 | 0.000 | 0.000 | 0.000 |
| | Jun | 0.000 | 0.000 | 0.000 | 0.000 | 0.000 |
| | Jul | 0.000 | 0.000 | 0.000 | 0.000 | 0.000 |
| | Aug | 0.000 | 0.000 | 0.000 | 0.000 | 0.000 |
| | Sep | 0.000 | 0.000 | 0.000 | 0.000 | 0.000 |
| | Oct | 0.000 | 0.000 | 0.000 | 0.000 | 0.000 |
| | Nov | 0.000 | 0.000 | 0.000 | 0.000 | 0.000 |
| | Dec | 0.000 | 0.000 | 0.000 | 0.000 | 0.000 |
| 2080s | Jan | 0.000 | 0.000 | 0.000 | 0.000 | 0.000 |
| | Feb | 0.000 | 0.000 | 0.000 | 0.000 | 0.000 |
| | Mar | 0.000 | 0.000 | 0.000 | 0.000 | 0.000 |
| | Apr | 0.000 | 0.000 | 0.000 | 0.000 | 0.000 |
| | May | 0.000 | 0.000 | 0.000 | 0.000 | 0.000 |
| | Jun | 0.000 | 0.000 | 0.000 | 0.000 | 0.000 |
| | Jul | 0.000 | 0.000 | 0.000 | 0.000 | 0.000 |
| | Aug | 0.000 | 0.000 | 0.000 | 0.000 | 0.000 |
| | Sep | 0.000 | 0.000 | 0.000 | 0.000 | 0.000 |
| | Oct | 0.000 | 0.000 | 0.000 | 0.000 | 0.000 |
| | Nov | 0.000 | 0.000 | 0.000 | 0.000 | 0.000 |
| | Dec | 0.000 | 0.000 | 0.000 | 0.000 | 0.000 |

changes lead to the increase in the probabilities of 30.9, 41.1 and 53.3 %, respectively. In contrast, the SDSM method predicts the smallest changes compared to the base years (1980s) of -2.7 % (2020s), -5.1 % (2050s) and 3.2 % (2080s), and has median values of 876.7, 855.1 and 930.1 mm, respectively. The variance changes are not the same as those of the median value. For the variances, the ASD method produces the largest changes (217.1, 146.1

and 263.4 mm²), while LarsWG5 shows the smallest changes (65.46, 70.08 and 80.80 mm²).

All the downscaling methods analyzed herein produce increases in the annual mean T_{\max} for the future years. The median value of T_{\max} for the base years (1980s) is 20.2 °C. From the results, the five downscaling methods show increases in the mean T_{\max} for the next 110 years. The annual mean T_{\max} values will increase with range between

Table 5 Results (p value) of the T test for the equality means of the observed and downscaled daily p at the 95 % confidence level

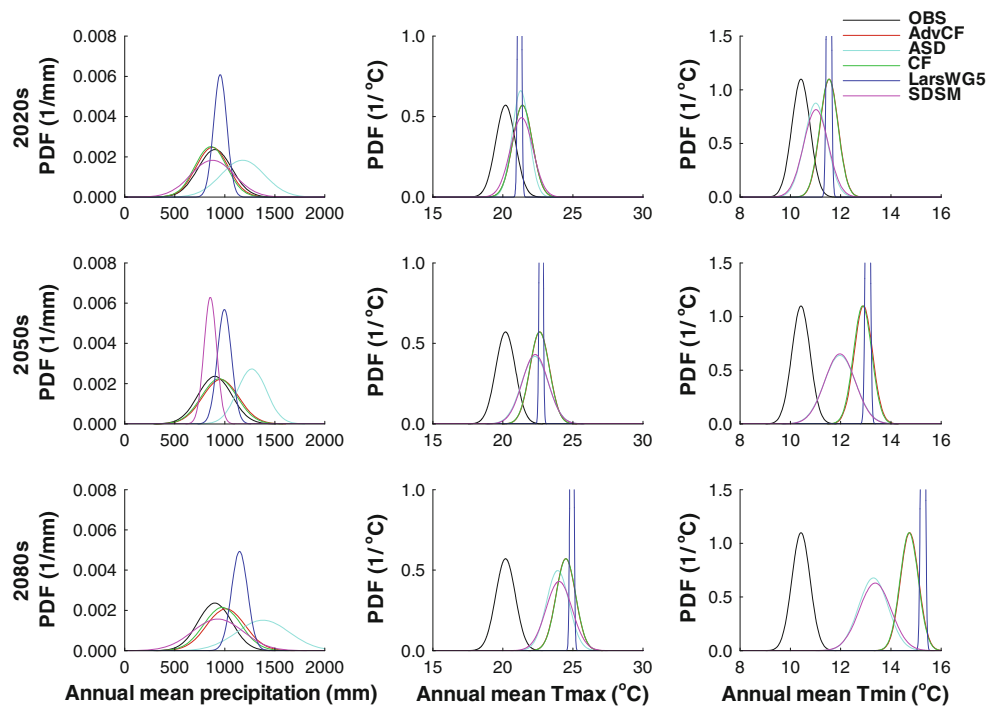
| Period | Month | p value | | | | |
|--------|-------|-----------|-------|-------|-------|---------|
| | | AdvCF | CF | ASD | SDSM | LarsWG5 |
| 2020s | Jan | 0.000 | 0.000 | 0.281 | 0.961 | 0.022 |
| | Feb | 0.000 | 0.000 | 0.000 | 0.165 | 0.048 |
| | Mar | 0.000 | 0.000 | 0.000 | 0.138 | 0.678 |
| | Apr | 0.000 | 0.000 | 0.000 | 0.100 | 0.251 |
| | May | 0.000 | 0.000 | 0.000 | 0.705 | 0.981 |
| | Jun | 0.000 | 0.000 | 0.000 | 0.642 | 0.112 |
| | Jul | 0.000 | 0.000 | 0.838 | 0.000 | 0.463 |
| | Aug | 0.000 | 0.000 | 0.013 | 0.256 | 0.846 |
| | Sep | 0.000 | 0.000 | 0.12 | 0.213 | 0.579 |
| | Oct | 0.000 | 0.000 | 0.000 | 0.061 | 0.193 |
| | Nov | 0.000 | 0.000 | 0.000 | 0.138 | 0.362 |
| | Dec | 0.000 | 0.000 | 0.000 | 0.022 | 0.168 |
| 2050s | Jan | 0.000 | 0.000 | 0.483 | 0.121 | 0.000 |
| | Feb | 0.000 | 0.000 | 0.000 | 0.020 | 0.000 |
| | Mar | 0.000 | 0.000 | 0.000 | 0.017 | 0.002 |
| | Apr | 0.000 | 0.000 | 0.000 | 0.018 | 0.004 |
| | May | 0.000 | 0.000 | 0.000 | 0.877 | 0.955 |
| | Jun | 0.000 | 0.000 | 0.014 | 0.010 | 0.622 |
| | Jul | 0.000 | 0.000 | 0.124 | 0.000 | 0.268 |
| | Aug | 0.000 | 0.000 | 0.963 | 0.374 | 0.357 |
| | Sep | 0.000 | 0.000 | 0.000 | 0.715 | 0.931 |
| | Oct | 0.000 | 0.000 | 0.000 | 0.019 | 0.707 |
| | Nov | 0.000 | 0.000 | 0.000 | 0.009 | 0.115 |
| | Dec | 0.000 | 0.000 | 0.000 | 0.000 | 0.001 |
| 2080s | Jan | 0.000 | 0.000 | 0.665 | 0.042 | 0.000 |
| | Feb | 0.000 | 0.000 | 0.000 | 0.005 | 0.000 |
| | Mar | 0.000 | 0.000 | 0.000 | 0.051 | 0.000 |
| | Apr | 0.000 | 0.000 | 0.000 | 0.021 | 0.000 |
| | May | 0.000 | 0.000 | 0.000 | 0.559 | 0.276 |
| | Jun | 0.000 | 0.000 | 0.004 | 0.143 | 0.521 |
| | Jul | 0.000 | 0.000 | 0.102 | 0.000 | 0.083 |
| | Aug | 0.000 | 0.000 | 0.791 | 0.000 | 0.001 |
| | Sep | 0.000 | 0.000 | 0.000 | 0.000 | 0.004 |
| | Oct | 0.000 | 0.000 | 0.000 | 0.286 | 0.000 |
| | Nov | 0.000 | 0.000 | 0.000 | 0.171 | 0.000 |
| | Dec | 0.000 | 0.000 | 0.000 | 0.000 | 0.000 |

3.7 and 4.7 °C. LarsWG5 provides the largest increase with a median value of 24.9 °C, while ASD has the smallest increase with a median value of 23.9 °C. The median values of the AdvCF, CF and SDSM methods are 24.5, 24.5 and 24.0 °C, respectively. In addition, SDSM shows the largest variance in the mean T_{\max} and LarsWG5 shows the smallest variance in the mean T_{\max} .

For the annual mean T_{\min} results, all the downscaling methods obtain the same increasing trend in the median

and variance values. The base years (1980s) have a median value of 10.4 °C and variance of 0.36 (°C)² for the annual mean T_{\min} values. In the following 110 years, the annual mean T_{\min} will increase with range between 2.9 and 4.9 °C. Results show that the LarsWG5 method produces the largest increase with a median value of 15.3 °C, while the ASD method shows the smallest increase with a median value of 13.3 °C. The median values for the AdvCF, CF and SDSM methods are 14.7, 14.7 and 13.4 °C,

Fig. 8 PDFs of annual mean precipitation, annual mean T_{max} and annual mean T_{min} for the base years (1980s, shown as the OBS data) and the future years (2020s, 2050s and 2080s)



respectively. Lastly, smallest variance in the annual mean T_{min} was found with the LarsWG5 method with a variance <0.1 ($^{\circ}C$)².

4.3 Hydrologic impacts of climate change

Figure 9 displays the monthly discharge results from the hydrologic model for the five downscaling methods for the future years (2020s, 2050s and 2080s). Results from the downscaling methods showed that most of peak values for the discharges are in the range of 4,000–5,000 m³/s; however, the ASD method showed a significant increase in the discharge results versus the other methods with some months producing a discharge of 10,000 m³/s. These differences in the discharges may be related to the different climatic scenarios (T_{max} , T_{min} and P); however, it should also be mentioned that the XAJ-RR model is sensitive to precipitation. Tiny changes in precipitation could lead to large fluctuations in the discharge values. Another reason for the differences in the discharges could be related to the A2 scenario used in this research being a high emission scenario, thus it makes large increases in temperature and precipitation as compared to the OBS for the future.

In regards to the annual mean discharges from the hydrologic model (results shown in Table 6), all of the five downscaling methods show increases in the discharge as compared to that of the base years. The ASD method produced the largest increase in the annual mean discharges during the three future periods with the percent

changes between the future and base years of 98.2, 97.3 and 82.3 %, respectively. While, the SDSM method provided the smallest increase in the discharge values with changes of 0.8, 3.2 and 7.6 % for the future years (2020s, 2050s and 2080s), respectively. These trends in the mean annual discharges are consistent with the trends shown for the precipitation. In looking at the results presented in Table 6, the ASD method results show an interesting trend of decrease in the changes between the future and base year, while the other downscaling methods all show the changes increasing over the future years. In addition, the AdvCF method produces larger increases in the changes than the CF method for each of the future periods.

In contrast, the variance results presented in Table 6 show a decreasing trend in the changes as compared to the mean results discussed earlier. Results show that only the ASD method obtains higher variances changes for the future years than those of the base years and that these changes decrease over the future years, while the other downscaling methods provide lower variances changes for the future years than the base years and have changes that increase over the future years.

Figure 10 presents the PDFs of the annual mean discharge for both the future years and the base years. The PDFs show the uncertainties and how they relate to downscaling methods. The annual mean discharge for the base years (1980s) is from 0 to 2,000 m³/s with a median value of 993.3 m³/s. Figure 10 shows that all of the downscaling methods produce increases in annual mean

Fig. 9 The discharges predicted for the future years (2020s, 2050s and 2080s) at the upstream portion of the Huaihe River basin. The abscissa shows 360 months for 30 years during the chose period

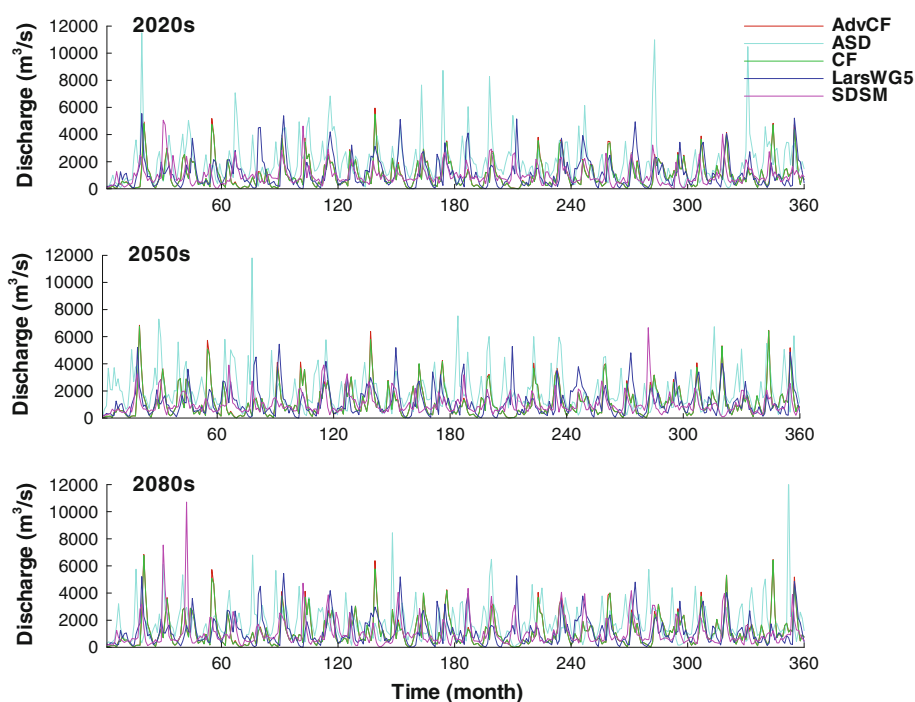


Table 6 Changes of annual mean discharge and variance for the future years (2020s, 2050s and 2080s) compared with the base years (1980 s)

| | Period | AdvCF | ASD | CF | LarsWG5 | SDSM |
|-----------------------------|--------|-------|------|-------|---------|-------|
| Mean increase value (%) | 2020s | 4.8 | 98.2 | 2.2 | 17.2 | 0.8 |
| | 2050s | 18.9 | 97.3 | 16.1 | 20.0 | 3.2 |
| | 2080s | 19.1 | 82.3 | 18.0 | 44.8 | 7.6 |
| Variance increase value (%) | 2020s | -19.4 | 55.3 | -21.0 | -20.3 | -35.7 |
| | 2050s | -9.2 | 22.7 | -10.9 | -17.3 | -46.8 |
| | 2080s | -6.4 | 13.9 | -9.9 | -6.2 | -29.1 |

discharge for the future years as compared to the base years. Results indicate that the ASD method provides the largest increases in the median values in the annual mean discharge with a range of 82.3–98.2 % in the future years, while the SDSM method produced the smallest increases in the median value in the future years, which varied from 0.8 to 7.6 %. The annual mean discharge results increase in magnitude in the follow order for the five downscaling methods: ASD, LarsWG5, AdvCF, CF and SDSM. Lastly, the mean and variance of annual mean discharge increase with time for each of the downscaling methods.

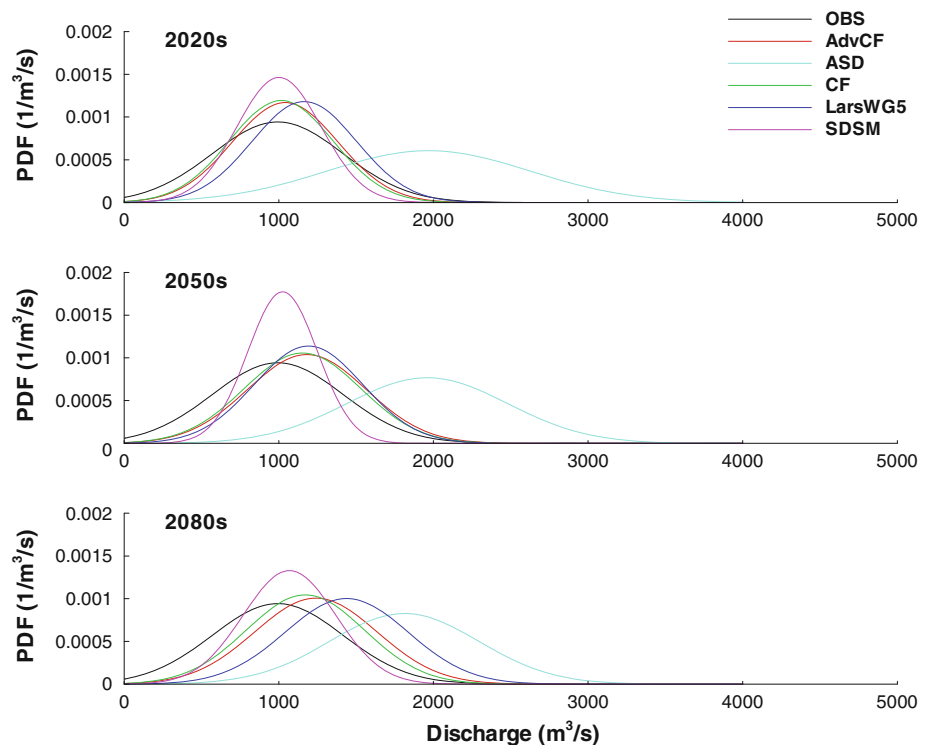
From the results presented in Fig. 10 it is evident that one cannot ignore uncertainty in the choice of the downscaling method utilized in determining the impact of climate change on the hydrology and water resources in a region. Each of the different downscaling methods provide different results, thus, the uncertainty with the downscaling methods can lead to uncertainties in the hydrological variables.

5 Discussion

Uncertainty is important when studying the impact of climate change on hydrology and water resources. Recently, many researchers have been examining the uncertainty in climate models, such as GCMs and GGES. The downscaling methods provide a tool to solving the mismatch scale issue between GCMs (large-scale) and hydrological models (small-scale). This area of research has enjoyed much development during the last two decades. The uncertainty in the downscaling methods introduces uncertainty in the hydrologic models.

Herein, five different downscaling methods are assessed for their impact of climate change on hydrology and water resources. A combination of the data from the HadCM3 model and the A2 scenario were used to investigate the uncertainty in the upstream portion of the Huaihe River basin in China. This paper examines the statistical variables of the regional climate scenarios (i.e. P , T_{\max} and

Fig. 10 PDFs of the annual mean discharge for the base years (1980s, shown as the OBS data) and the future years (2020s, 2050s and 2080s)



T_{\min}) produced by the five downscaling methods to investigate their uncertainty. For instance, the statistical variables investigated within this study for the future years (2020s, 2050s and 2080s) were: daily precipitation, monthly mean T_{\max} and T_{\min} , POT and PBT, changes of T_{\max} and precipitation with seasons, error evaluation in the estimates of means between the base years and the future years, and PDF of three predictants. Paired-sample *T*-test was used to estimate the significance at the 95 % significant level.

All of the downscaling methods suggest increases in temperature for the future years. This conclusion is the same as previous studies'. But Chen et al. (2011a) presented temperature (average of T_{\max} and T_{\min}) increases range between 3.6 and 6.3 °C for spring, 0.4 and 4.1 °C for summer, 1.8 and 4.8 °C for autumn and between 5.7 and 9.1 °C for winter, which concluded that the winter temperature increase were greater than for others in Canada for the 2,085 horizon in Canada. While this paper concluded that the summer temperature (T_{\max}) increase are greater than other seasons in the upstream portion of the Huaihe River Basin for 2080s, increases range between 2.8 and 4.3 °C for spring, 5.2 and 6.8 °C for summer, 3.0 and 5.1 °C for autumn and between 2.7 and 4.2 °C for winter. Gao et al. (2010) used ANN to project streamflow derived from the ECHAM5/MPI-OM model under three emission scenarios (A2, A1B and B1) in the same area and the same period with this study. The interannual fluctuations of streamflow displayed a relatively significant increasing

trend under the SRES-A2 scenario, especially from 2051 to 2085. It was projected that the runoff of the Huaihe River fluctuates significantly in the future and would decrease in the end of twenty first century. But their study used a single downscaling model. In this paper, five downscaling methods display a relatively increasing trend of discharge derived from the HadCM3 model under A2 scenario. The overall results of the ASD method suggest the largest increase (82.3 %) and the SDSM method suggest the least increase (7.6 %) in the 2080s. This projection is in line with the increasing precipitation, the ASD method suggests the largest increase (53.3 %) and the SDSM method suggests the least increase (3.2 %) in the 2080s. Khan et al. (2006b) investigated the uncertainty of downscaling methods by non-parametric test at two meteorological stations in the current, while this paper test it over the basin in the future. The results of this paper are more significant in many months due to the climate change in the future. In this paper, POT and PBT of observed in the base years and downscaled in the future years are compared to demonstrate the increasing of temperature in the other view, which indicate the uncertainty of downscaling methods too.

This paper takes a multifaceted view of the uncertainties of downscaling methods. These results illustrate that the uncertainties shown in hydrological variables are related to those that are produced with the downscaling methods. It is demonstrated that interpreting and using the output of only one downscaling method are need for extreme caution.

There are many factors cause the uncertainties of downscaling methods: (1) Method uncertainties due to structural errors of the downscaling methods. (2) Method uncertainties due to processes of screen predictors; for example, a partial correlation analysis is applied in SDSM method and a stepwise linear regression approach is used in ASD method, only strong correlation with predictants are take into account. (3) Method uncertainties due to processes of variance inflation and bias correction, for example, which were set automatically in ASD and set manually in SDSM. (4) Method uncertainties due to different optimal algorithms used to calculate parameters. (5) Method uncertainties due to resolution of GCM outputs in the future, for example, IDW was utilized to interpolate the GCM outputs in AdvCF method. This paper takes a multifaceted view of the uncertainties of downscaling methods. Compared with previous studies, the results are more obvious and the reasons are more fully.

6 Conclusions

Five downscaling methods were used to investigate the uncertainty of downscaling methods. Regional climate scenarios and hydrological variables projected by five methods were presented above. The comparative downscaling results show that uncertainties exist in downscaling methods. All the studies about climate change based on a single downscaling method should be caution. The uncertainty about downscaling methods should be pay attention to as GCMs and GGES.

Because of the uncertainties in the GCMs, emission scenarios, downscaling methods and hydrological models, the errors are inevitable between simulations and OBSs of predictands. The A2 scenarios assume a high population growth, which results in higher emission. The A2 scenario has high emissions than the other scenarios defined by IPCC, which is due to the assumption of rapid population growth. Therefore, the downscaling methods for the A2 scenario would produce the largest changes than the other emissions scenarios. All five downscaling methods were found to predict an increase in T_{\max} by 2080s as compared to the OBS of the 1980s, with the range of the changes between 3.7 and 4.7 °C. In the case of T_{\min} , these changes ranged between 2.8 and 4.9 °C. These increases in T_{\max} and T_{\min} would be reduced if the A2 emission scenario were replaced with the other low-emission scenarios. Results indicate that all the downscaling methods produce varying increases in the annual mean precipitation by 2080s, which range between 3.2 and 53.3 %.

The output from the model, HadCM3, was downscaled by the five methods discussed herein to produce different future regional climate change scenarios. These results

were then utilized in the XAJ-RR model to predict the hydrological changes in the Huaihe River basin. The XAJ-RR model employs precipitation, evapotranspiration and 15 model parameters to produce discharge information. The evapotranspiration is relevant to T_{\max} and T_{\min} variables. Results from the hydrology model show that the choice of downscaling methods plays a significant role in accurately capturing the impacts of climate change, and that the uncertainty present in the downscaling methods leads to uncertainty in the results from the hydrology models.

Several assumption were utilized in determining the impact of climate change on the hydrology and water resources in the Huaihe River basin, thus the results presented herein can only be used to provide forecasts or some guidance. The downscaling methods must be chosen in a deliberate fashion, as these methods are just as important to assessing the impact of climate change on the hydrology as choosing the GCMs and GGES. The accurate evaluation of the impact of climate change is important for the planning and management of the water resources in the future.

Acknowledgments This research is supported by the Program for National Basic Research Program of China (2013CBA01806, 2010CB951101), the Major Program of National Natural Science Foundation of China (51190090), NSSF (41371049, 50939006), the Program for Graduate Education Innovation Project in Jiangsu Province (CXLX13_239) and IWHRSKL-201213. The authors wish to acknowledge gratefully Kendra M. Dresback of University of Oklahoma for revising the grammar of this paper.

References

- Arora VK, Boer GJ (2001) Effects of simulated climate change on the hydrology of major river basins. *J Geophys Res* 106(D4): 3335–3348
- Bárdossy A, Stehlík J, Caspary H-J (2002) Automated objective classification of daily circulation patterns for precipitation and temperature downscaling based on optimized fuzzy rules. *Clim Res* 23:11–22
- Bastola S, Murphy C, Sweeney J (2011) The role of hydrological modelling uncertainties in climate change impact assessments of Irish river catchments. *Adv Water Resour* 34(5):562–576
- Boé J, Terray L, Habets F, Martin E (2006) A simple statistical-dynamical downscaling scheme based on weather types and conditional resampling. *J Geophys Res Atmos* 111(D23). doi: [10.1029/2005JD006889](https://doi.org/10.1029/2005JD006889)
- Charlton R, Fealy R, Moore S, Sweeney J, Murphy C (2006) Assessing the impact of climate change on water supply and flood hazard in Ireland using statistical downscaling and hydrological modelling techniques. *Clim Chang* 74(4):475–491
- Chen J, Brissette FP, Leconte R (2011a) Uncertainty of downscaling method in quantifying the impact of climate change on hydrology. *J Hydrol* 401(3–4):190–202
- Chen J, Brissette FP, Poulin A, Leconte R (2011b) Overall uncertainty study of the hydrological impacts of climate change for a Canadian watershed. *Water Resour Res* 47(12):W12509
- Christensen NS, Wood AW, Voisin N, Lettenmaier DP, Palmer RN (2004) The effects of climate change on the hydrology and water

- resources of the Colorado river basin. *Clim Chang* 62(1): 337–363
- Chu J, Xia J, Xu CY, Singh V (2010) Statistical downscaling of daily mean temperature, pan evaporation and precipitation for climate change scenarios in Haihe River, China. *Theor Appl Climatol* 99(1):149–161
- Conway D, Jones PD (1998) The use of weather types and air flow indices for GCM downscaling. *J Hydrol* 212–213:348–361
- Diaz-Nieto J, Wilby R (2005) A comparison of statistical downscaling and climate change factor methods: impacts on low flows in the River Thames, United Kingdom. *Clim Chang* 69(2–3): 245–268
- Dibike YB, Coulibaly P (2005) Hydrologic impact of climate change in the Saguenay watershed: comparison of downscaling methods and hydrologic models. *J Hydrol* 307(1–4):145–163
- DíEz E, Primo C, GarcÍA-Moya JA, GutiÉRrez JM, Orfila B (2005) Statistical and dynamical downscaling of precipitation over Spain from DEMETER seasonal forecasts. *Tellus A* 57(3): 409–423
- Ebrahim GY, Jonoski A, Griensven Av, Baldassarre GD (2012) Downscaling technique uncertainty in assessing hydrological impact of climate change in the Upper Beles River Basin, Ethiopia. *Hydrol Res* 43. doi:10.2166/nh.2012.037
- Enke W, Spekat A (1997) Downscaling climate model outputs into local and regional weather elements by classification and regression. *Clim Res* 8:195–207
- Fedderson H, Andersen U (2005) A method for statistical downscaling of seasonal ensemble predictions. *Tellus A* 57(3):398–408
- Gao C, Gemmer M, Zeng X, Liu B, Su B, Wen Y (2010) Projected streamflow in the Huaihe River Basin (2010–2100) using artificial neural network. *Stoch Environ Res Risk Assess* 24(5):685–697
- Gleick PH (1989) Climate change, hydrology, and water resources. *Rev Geophys* 27(3):329–344
- Gordon C, Cooper C, Senior CA, Banks H, Gregory JM, Johns TC, Mitchell JFB, Wood RA (2000) The simulation of SST, sea ice extents and ocean heat transports in a version of the Hadley Centre coupled model without flux adjustments. *Clim Dyn* 16(2–3):147–168
- Hargreaves GH, Samani ZA (1982) Estimating potential evapotranspiration. *J Irrig Drain Div* 108(3):225–330
- Hay LE, Wilby RL, Leavesley GH (2000) A comparison of delta change and downscaled GCM scenarios for three mountainous basins in the United States. *JAWRA J Am Water Resour Assoc* 36(2):387–397
- Haylock MR, Cawley GC, Harpham C, Wilby RL, Goodess CM (2006) Downscaling heavy precipitation over the United Kingdom: a comparison of dynamical and statistical methods and their future scenarios. *Int J Climatol* 26(10):1397–1415
- Herrmann MJ, Somot S (2008) Relevance of ERA40 dynamical downscaling for modeling deep convection in the Mediterranean Sea. *Geophys Res Lett* 35(4). doi:10.1029/2007GL032442
- Hessami M, Gachon P, Ouarda TBMJ, St-Hilaire A (2008) Automated regression-based statistical downscaling tool. *Environ Model Softw* 23(6):813–834
- Huth R (1997) Potential of continental-scale circulation for the determination of local daily surface variables. *Theor Appl Climatol* 56(3):165–186
- Khan MS, Coulibaly P, Dibike Y (2006a) Uncertainty analysis of statistical downscaling methods. *J Hydrol* 319(1–4):357–382
- Khan MS, Coulibaly P, Dibike Y (2006b) Uncertainty analysis of statistical downscaling methods using Canadian Global Climate Model predictors. *Hydrol Process* 20(14):3085–3104
- Kiely G (1999) Climate change in Ireland from precipitation and streamflow observations. *Adv Water Resour* 23(2):141–151
- Leavesley GH (1994) Modeling the effects of climate change on water resources—a review. *Clim Chang* 28(1):159–177
- Lü H, Hou T, Horton R, Zhu Y, Chen X, Jia Y, Wang W, Fu X (2013) The streamflow estimation using the Xinanjiang rainfall runoff model and dual state-parameter estimation method. *J Hydrol* 480:102–114
- Ludwig R, May I, Turcotte R, Vescovi L, Braun M, Cyr J-F, Fortin L-G, Chaumont D, Biner S, Chartier I, Caya D, Mauser W (2009) The role of hydrological model complexity and uncertainty in climate change impact assessment. *Adv Geosci* 21:63–71
- Maurer E (2007) Uncertainty in hydrologic impacts of climate change in the Sierra Nevada, California, under two emissions scenarios. *Clim Chang* 82(3):309–325
- Merritt WS, Alila Y, Barton M, Taylor B, Cohen S, Neilsen D (2006) Hydrologic response to scenarios of climate change in sub watersheds of the Okanagan basin, British Columbia. *J Hydrol* 326(1–4):79–108
- Minville M, Brissette F, Leconte R (2008) Uncertainty of the impact of climate change on the hydrology of a nordic watershed. *J Hydrol* 358(1–2):70–83
- Najac J, Lac C, Terray L (2011) Impact of climate change on surface winds in France using a statistical-dynamical downscaling method with mesoscale modelling. *Int J Climatol* 31(3):415–430
- Nakicenovic N, Alcamo J, Davis G, de Vries B, Fenhann J, Gaffin S, Gregory K, Grubler A, Jung TY, Kram T, La Rovere EL, Michaelis L, Mori S, Morita T, Pepper W, Pitcher HM, Price L, Riahi K, Roehrl A, Rogner H-H, Sankovski A, Schlesinger M, Shukla P, Smith SJ, Swart R, van Rooijen S, Victor N, Dadi Z (2000) Special report on emissions scenarios: a special report of working Group III of the Intergovernmental panel on climate change
- Pinto JG, Neuhaus CP, Leckebusch GC, Reyers M, Kerschgens M (2010) Estimation of wind storm impacts over Western Germany under future climate conditions using a statistical-dynamical downscaling approach. *Tellus A* 62(2):188–201
- Pope VD, Gallani ML, Rowntree PR, Stratton RA (2000) The impact of new physical parametrizations in the Hadley Centre climate model: HadAM3. *Clim Dyn* 16(2–3):123–146
- Qi ZF, Ye XY, Zhang H, Yu, ZL (2013) Land fragmentation and variation of ecosystem services in the context of rapid urbanization: the case of Taizhou city, China. *Stoch Environ Res Risk Assess* 1–13. doi:10.1007/s00477-013-0721-2
- Quintana Seguí P, Ribes A, Martin E, Habets F, Boé J (2010) Comparison of three downscaling methods in simulating the impact of climate change on the hydrology of Mediterranean basins. *J Hydrol* 383(1–2):111–124
- Racsko P, Szeidl L, Semenov M (1991) A serial approach to local stochastic weather models. *Ecol Model* 57(1–2):27–41
- Risbey JS, Entekhabi D (1996) Observed Sacramento Basin streamflow response to precipitation and temperature changes and its relevance to climate impact studies. *J Hydrol* 184(3–4):209–223
- Semenov MA, Brooks RJ, Barrow EM, Richardson CW (1998) Comparison of the WGEN and LARS-WG stochastic weather generators for diverse climates. *Clim Res* 10(2):95–107
- Singh K, Xie M (2008) Bootstrap: a statistical method. www.stat.rutgers.edu/~mxie/rcpapers/bootstrap.pdf
- Steele-Dunne S, Lynch P, McGrath R, Semmler T, Wang S, Hanafin J, Nolan P (2008) The impacts of climate change on hydrology in Ireland. *J Hydrol* 356(1–2):28–45
- Tatli H, Nüzhet Dalfes H, Sibel Menteş Ş (2004) A statistical downscaling method for monthly total precipitation over Turkey. *Int J Climatol* 24(2):161–180
- Vicuna S, Maurer EP, Joyce B, Dracup JA, Purkey D (2007) The sensitivity of California water resources to climate change scenarios. *JAWRA J Am Water Resour Assoc* 43(2):482–498

- Wang T, Istanbuluoglu E, Lenters J, Scott D (2009) On the role of groundwater and soil texture in the regional water balance: an investigation of the Nebraska Sand Hills, USA. *Water Resour Res* 45(10):W10413
- Whitfield PH, Cannon AJ (2000) Recent variations in climate and hydrology in Canada. *Can Water Resour J* 25(1):19–65
- Wilby RL, Wigley TML (1997) Downscaling general circulation model output: a review of methods and limitations. *Prog Phys Geogr* 21(4):530–548
- Wilby RL, Hay LE, Leavesley GH (1999) A comparison of downscaled and raw GCM output: implications for climate change scenarios in the San Juan River basin, Colorado. *J Hydrol* 225(1–2):67–91
- Wilby RL, Dawson CW, Barrow EM (2002) SDSM—a decision support tool for the assessment of regional climate change impacts. *Environ Model Softw* 17(2):147–159
- Wilby RL, Tomlinson OJ, Dawson CW (2003) Multi-site simulation of precipitation by conditional resampling. *Clim Res* 23(3): 183–194
- Xu CY (1999) Climate change and hydrologic models: a review of existing gaps and recent research developments. *Water Resour Manag* 13(5):369–382
- Yue W, Liu Y, Fan P, Ye X, Wu C (2012) Assessing spatial pattern of urban thermal environment in Shanghai, China. *Stoch Environ Res Risk Assess* 26(7):899–911
- Zhao RJ (1992) The Xinanjiang model applied in China. *J Hydrol* 135(1–4):371–381
- Zhao RJ, Zhang YL, Fang LR (1980) The Xinanjiang model. In: *Hydrological forecasting proceedings of oxford symposium IASH*, vol 129, pp. 351–356